The combined effect of optical laser and microwave radiations on a metal surface

Anatoli P Gavrilyuk[a)b)] and Nikolai Ya Shaparev[a)†]

[a)] *Institute of Computational Modeling of Siberian Branch of Russian Academy of Sciences, Akademgorodok, Krasnoyarsk, Russia*
[b)] *Siberian Federal University, Krasnoyarsk, Russia*

(Received 19 April 2013; revised manuscript received 6 June 2013; published online 20 December 2013)

In this paper, it is shown that the laser radiation intensity required for complete ionization of vapors produced on an irradiated metal surface can be reduced by more than an order of magnitude through using pulsed laser radiation in combination with microwave radiation.

Keywords: laser, microwave radiation, metal surface, plasma

PACS: 52.38.Mf, 52.50.Jm, 52.25.Os **DOI:** 10.1088/1674-1056/23/2/025205

1. Introduction

It is known that a microwave field (10^9 s$^{-1} \leq \omega_m \leq 10^{12}$ s^{-1}) is effectively reflected from a metal surface. Because of this, the application of a microwave field cannot result in heating and vaporization of the metal surface whereas optical laser irradiation does lead to metal heating, melting, and vaporization.[1] However, if the laser radiation intensity is not high enough or the pulse duration is not long enough, then the resulting plasma will be weakly ionized.

Absorption of microwave radiation (MR) in a weakly ionized gas is higher than absorption of laser radiation. So, a microwave field applied to the metal surface causes additional heating and ionization of vapors produced by laser irradiation. Consequently, the optical radiation absorption is also increased due to inverse bremsstrahlung, resulting in turn in additional electron heating and enhanced ionization, which can lead to electron avalanche ignition and full vapor ionization.

Being able to control plasma formation is important, both for studying interaction of laser radiation with metals and for laser and plasma treatment of metals.[2]

2. Model

An investigation of the above processes has been performed in terms of the approach described in Ref. [3]. We study the heating, melting, and vaporization of the target under applied laser radiation as well as the subsequent heating and ionization of the resultant vapors in the laser field.

In our study we also take into consideration the MR interaction with the vapor layer. The model includes a one-dimensional heat conduction equation for an area with an undefined flat-plate moving boundary that separates the solid ($i = S$) and liquid ($i = L$) phases from each other (Fig. 1)

$$\rho_i(T)C_i(T)\frac{\partial T_i}{\partial t} = \frac{\partial}{\partial x}\left(\lambda(T)\frac{\partial T}{\partial x}\right)_i, \quad i = S,\ L, \tag{1}$$

where T is the temperature, $\rho_i(T)$ is the density, $C_i(T)$ is the heat capacity, and $\lambda_i(T)$ is the thermal conductivity. At the solid–liquid phase transition boundary (Γ), the Stephan condition and the temperature equality are satisfied:

$$\lambda_L\frac{\partial T_L}{\partial x} - \lambda_S\frac{\partial T_S}{\partial x} = \rho_S L_\mathrm{m} V_\mathrm{m}, \quad T_\mathrm{m} = T_L = T_S, \tag{2}$$

where L_m, T_m, and V_m are the specific heat of fusion and the melting front temperature and velocity, respectively.

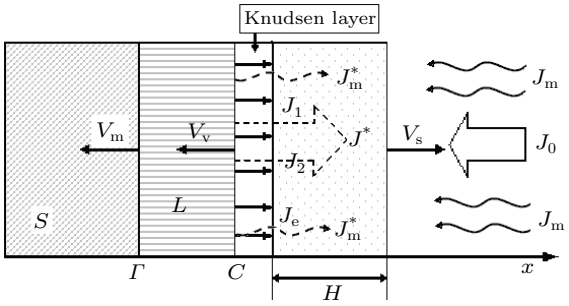


Fig. 1. A diagram of the metal surface exposure to the radiations.

Equations (1) and (2) should be supplemented by the boundary condition on the metal surface through taking into account the thermal flow balance:

$$\lambda_L\frac{\partial T_L}{\partial x} = \rho_L L_\mathrm{v} V_\mathrm{v} - r_\mathrm{c} J^+, \tag{3}$$

where L_v is the specific heat of vaporization; V_v is the velocity of the vaporization front; J^+ is the intensity of the radiation passed through the vapor layer and incident on the metal surface, r_c is the coefficient of laser radiation absorption by the metal surface.

To describe the phase transition between the condensed medium (boundary C in Fig. 1) and the vapor layer, we employ the Knight evaporation model[4] where the gas dynamic properties of vapors at the Knudsen layer boundary are derived

†Corresponding author. E-mail: shaparev@icm.krasn.ru

© 2014 Chinese Physical Society and IOP Publishing Ltd

from the equations of mass flow, pulse and energy conservation. The thickness of the Knudsen layer (Fig. 1) is several times the mean free path of vapor atoms. The velocity distribution function of atoms in this layer is semi-Maxwellian (non-equilibrium) turning equilibrium outside this layer. In terms of gas dynamics, the Knudsen layer is a region of strong discontinuity. The temperature of particles evaporated from this layer is lower than the surface temperature because part of their thermal energy is converted into kinetic energy of the gas flow. This is one of the important features of the model, which is distinct from the isothermal jump approach used in Ref. [5]. In the latter approach the surface temperature and the temperature of the adjacent vapor layer are assumed to be equal, which is only valid for saturated vapor confined to the surface. The inadequacy of the isothermal jump model was pointed out in Refs. [4] and [6].

The relation between the surface temperature and the temperature of vapors outflowing from the Knudsen layer, as well as between their density and that of saturated vapors, is given by[4]

$$
\begin{aligned}
&p_{\rm k} = \rho_{\rm k} R_{\rm g} T_{\rm k}, \quad p_* = \rho_* R_{\rm g} T_{\rm c}, \quad u_{\rm k} = M_{\rm m}\sqrt{\gamma_{\rm a} R_{\rm g} T_{\rm k}},\\
&T_{\rm k} = T_{\rm c}\left[\sqrt{1+\left(\frac{\sqrt{\pi}}{8}m_{\rm s}\right)^2} - \frac{\sqrt{\pi}}{8}m_{\rm s}\right]^2, \quad m_{\rm s} = \sqrt{\frac{\gamma_{\rm a}}{2}}M_{\rm m},\\
&\rho_{\rm k} = \rho_*\left\{\sqrt{\frac{T_{\rm c}}{T_{\rm k}}}\left[m_{\rm s}^2 + \frac{1}{2}\exp(m_{\rm s}^2)\operatorname{erfc}(m_{\rm s}) - \frac{m_{\rm s}}{\sqrt{\pi}}\right]\right.\\
&\qquad \left. + \frac{1}{2}\frac{T_{\rm c}}{T_{\rm k}}\left[1 - \sqrt{\pi}m_{\rm s}\exp(m_{\rm s}^2)\operatorname{erfc}(m_{\rm s})\right]\right\}. \qquad (4)
\end{aligned}
$$

Here, $R_{\rm g} = k_{\rm B}/M$ is the gas constant, with $k_{\rm B}$ is the Boltzmann constant, and M is the atom mass; $M_{\rm m}$ is the Mach number; $T_{\rm k}$, $\rho_{\rm k}$, $u_{\rm k}$ are the temperature, density, and velocity of the gas leaving the Knudsen layer; ρ_* and p_* are the saturated vapor density and pressure; $\gamma_{\rm a}$ is the adiabatic exponent ($\gamma_{\rm a} = 5/3$), and $T_{\rm c}$ is the metal surface temperature. When the ambient gas pressure is $p_0 \ll p_*$ (which is the case in our study), $M_{\rm m} \approx 1$.[4,6] Hence, from Eq. (4) we obtain simple expressions as follows:

$$
u_{\rm k} = \sqrt{\gamma_{\rm a} R_{\rm g} T_{\rm k}}, \quad T_{\rm k} \approx 0.67 T_{\rm c}, \quad \text{and} \quad \rho_{\rm k} \approx 0.86\rho_*.
$$

Processes occurring in the gaseous medium are described using the model within which variables (concentration, temperature, etc.) are averaged over the entire gaseous medium having the size H (Fig. 1). In turn, H is determined by the external boundary moving at the speed of sound

$$
V_{\rm s} = \sqrt{\gamma_{\rm a} k_{\rm B} T/M}, \qquad (5)
$$

where T is the temperature of atoms and ions.

The atom is treated as a three-level system comprising the ground (1), excited (2), and ionized (e) state. The temperatures of heavy particles (atoms and ions) are assumed to be equal. The kinetics of plasma formation is described by the following set of equations:

$$
\begin{aligned}
&\frac{{\rm d}H}{{\rm d}t} = V_{\rm s},\\
&\frac{{\rm d}n_{\rm e}}{{\rm d}t} = \frac{j_{\rm e}}{H} - n_{\rm e}\frac{\dot{H}}{H} + S_2 n_2 n_{\rm e} + S_1 n_1 n_{\rm e} - R_1 n_{\rm e}^3 - R_2 n_{\rm e}^3,\\
&\frac{{\rm d}n_1}{{\rm d}t} = \frac{j_1}{H} - n_1\frac{\dot{H}}{H} + K_{21} n_2 n_{\rm e} + A_{21}^* n_2 + R_1 n_{\rm e}^3 - K_{12} n_1 n_{\rm e}\\
&\qquad - S_1 n_1 n_{\rm e}, \quad A_{21}^* = \frac{A_{21}}{\sqrt{\pi\sigma n_1 H/2}},\\
&\frac{{\rm d}n_2}{{\rm d}t} = \frac{j_2}{H} - n_2\frac{\dot{H}}{H} - S_2 n_2 n_{\rm e} - A_{21}^* n_2 - K_{21} n_2 n_{\rm e}\\
&\qquad + K_{12} n_1 n_{\rm e} + R_2 n_{\rm e}^3,\\
&\frac{{\rm d}T_{\rm e}}{{\rm d}t} = \frac{j_{\rm e}}{H n_{\rm e}}\left(T_{\rm k} - T_{\rm e}\right) + \frac{2}{3k_{\rm B}}\mu_{\rm b}\frac{J}{n_{\rm e}} + \frac{2}{3}\cdot\frac{(1-r_{\rm m})}{H n_{\rm e}}J_{\rm m}\\
&\qquad + \frac{2}{3k_{\rm B}}E_{12}\left(K_{21} n_2 - K_{12} n_1\right)\\
&\qquad + \left(T_{\rm e} + \frac{2}{3k_{\rm B}}I_1\right)\left(R_1 n_{\rm e}^2 - S_1 n_2\right)\\
&\qquad + \left(T_{\rm e} + \frac{2}{3k_{\rm B}}I_2\right)\left(R_2 n_{\rm e}^2 - S_2 n_2\right) - C_{\rm e}\left(T_{\rm e} - T\right),\\
&\frac{{\rm d}T}{{\rm d}t} = C_{\rm e}\frac{n_{\rm e}}{n_1+n_2}(T_{\rm e} - T) + \left(\frac{j_1+j_2}{n_1+n_2}\right)\cdot\left(\frac{T_{\rm k}-T}{H}\right),\\
&\mu_{\rm b} \approx 0.1\cdot n_{\rm e}\frac{\nu_{\rm ea}+\nu_{\rm ei}}{\omega_0^2}, \quad C_{\rm e} = C_{\rm ea} + C_{\rm ei}, \quad C_{\rm ea} \approx \frac{2m}{M}\nu_{\rm ea},\\
&C_{\rm ei} \approx \frac{2m}{M}\nu_{\rm ei}. \qquad (6)
\end{aligned}
$$

Here n_1, n_2, and $n_{\rm e}$ are the concentrations of unexcited and excited atoms and electrons, respectively; $T_{\rm e}$ is the temperature of electrons; S_1 and S_2 are the ionization rate coefficients of normal and excited atoms induced by electron impact, respectively; E_{12} is the excitation energy of the atom; I_1 and I_2 denote the ionization potentials from the ground and excited states, respectively; K_{12} and K_{21} are the excitation and de-excitation rate coefficients under electron impact; R_1 and R_2 are the coefficients of a three-body recombination to the ground and excited states; A_{21}^* is the effective coefficient of spontaneous decay of excited atoms determined for a flat layer of H thickness as in Ref. [7]; A_{21} is the rate of spontaneous decay of an atom; m is the mass of electron; $\mu_{\rm b}$ is the inverse bremsstrahlung laser absorption coefficient;[8] ω_0 is the laser radiation frequency; $C_{\rm e}$ denotes the elastic energy exchange between electron and heavy particle; $\nu_{\rm ea}$ and $\nu_{\rm ei}$ are the electron–atom and electron–ion collision frequency; j_1 and j_2 are the flux of evaporated unexcited and excited atoms and electrons, respectively; $j_{\rm e}$ is the flux of electrons. The second and the third terms in the temperature equation $T_{\rm e}$ account for the heating of electrons, respectively, by laser and MR due to inverse bremsstrahlung absorption. In that equation, $r_{\rm m}$ is the

coefficient of MR reflection from ionized medium to be determined later and J_m is the MR intensity. The first term on the right-hand side of the second expression in Eq. (6) is responsible for the inflow of electrons due to thermal emission from the metal surface while the second one accounts for reduced concentration of electrons resulting from expansion of the gaseous layer. The same considerations are applied to the concentration of atoms. When determining the particle flows j_2 and j_e, we assume the Boltzmann ratio and the Saha equation to be satisfied for these particles at the temperature T_k at the Knudsen layer boundary; the quasi-neutrality condition is also assumed to be satisfied ($j_i \approx j_e$, j_i is the density of the ion flux). We then have

$$j_1 + j_2 + j_e = \frac{\rho_k u_k}{M}, \quad \frac{j_2}{j_1} = \frac{g_2}{g_1}\exp\Big(-\frac{E_{12}}{k_B T_k}\Big),$$
$$\frac{j_e^2}{j_1} = 2\Big(\frac{m_e k_B T_k}{2\pi\hbar^2}\Big)^{3/2}\frac{g_i}{g_1}\exp\Big(-\frac{I_1}{k_B T_k}\Big). \tag{7}$$

The average intensity J across the thickness of the gas layer H comprised of the set of equations (6) is found from the quasistationary transfer equation $\mathrm{d}J/\mathrm{d}x = -\mu_b J$ with mean concentration values:

$$J = \frac{J_0 + J^+ + J^* + J^-}{2}, \quad J^+ = J_0\exp\big(-\mu_b H\big),$$
$$J^* = J^+\big[1 - r_c(T_c)\big], \quad J^- = J^*\exp\big(-\mu_b H\big). \tag{8}$$

Here, the following intensity notations have been used: J_0 for the input laser radiation; J^+ for radiation passing through the layer H and incident on the surface; J^* for radiation reflected from the surface; J^- for radiation leaving the H layer. Successful application of this model to the description of experimental results on UV irradiation of an aluminum surface[5] was reported in Ref. [9]. Moreover, this model enables us to predict the effect of the screening of the target by the resulting plasma[3], which is later confirmed in the experiments on a lithium target.[10,11]

We now deal with the heating of electrons by MR. Part of this radiation penetrates the vapor layer, while part of the radiation is reflected from it. The reflection coefficient r_m is dependent on the thickness of the layer H, its complex dielectric permeability ε, the vapor density, and the extent of vapor ionization. For a given H, the coefficient r_m can be obtained as follows:[12]

$$r_m = \Big|\Big[\frac{1-\sqrt{\varepsilon}}{1+\sqrt{\varepsilon}}\exp(2\mathrm{i}\phi) - 1\Big] \Big/ \Big[\exp(2\mathrm{i}\phi) - \frac{1-\sqrt{\varepsilon}}{1+\sqrt{\varepsilon}}\Big]\Big|^2,$$
$$\phi = \frac{\omega_m}{c}H\sqrt{\varepsilon}, \quad \sqrt{\varepsilon} = \mu + \mathrm{i}\chi,$$
$$\mu = \Big\{0.5\Big(1 - \frac{\omega_p^2}{\omega_m^2 + \nu_{ea}^2}\Big) + 0.5\Big[\Big(1 - \frac{\omega_p^2}{\omega_m^2 + \nu_{ea}^2}\Big)^2 + \Big(\frac{\omega_p^2}{\omega_m^2 + \nu_{ea}^2}\cdot\frac{\nu_{ea}}{\omega_m}\Big)^2\Big]^{1/2}\Big\}^{1/2},$$
$$\chi = \Big\{-0.5\Big(1 - \frac{\omega_p^2}{\omega_m^2 + \nu_{ea}^2}\Big) + 0.5\Big[\Big(1 - \frac{\omega_p^2}{\omega_m^2 + \nu_{ea}^2}\Big)^2 + \Big(\frac{\omega_p^2}{\omega_m^2 + \nu_{ea}^2}\cdot\frac{\nu_{ea}}{\omega_m}\Big)^2\Big]^{1/2}\Big\}^{1/2},$$
$$\omega_p = \sqrt{\frac{4\pi e^2 n_e}{m}} = 5.65\cdot 10^4\sqrt{n_e}, \tag{9}$$

where c is the light velocity, ω_p is the plasma oscillation frequency, and ω_m is the MR frequency.

When being heated, the target evaporates, releasing atoms and electrons, whose concentration can be estimated from the Saha equation. Electrons are heated by laser radiation due to inverse bremsstrahlung absorption and excite the atoms. This is followed by a spontaneous decay of the atoms that lose their energy received from electrons. The situation, however, changes once the electron concentration n_e exceeds n_e^* determined as:

$$K_{21} n_e^* = A_{21}^*. \tag{10}$$

In this case, de-excitation of atoms is carried out predominantly by electrons. This means that the energy expended by electrons on excitation of atoms feeds back to the electron subsystem, and the channel of loss of the electron energy associated with spontaneous decay is of little importance. Our estimates (for $\lambda \approx 1$ μm within this model) suggest that for condition (10) to be satisfied at atomic concentrations $n \sim 10^{17}\div 10^{19}$ cm^{-3}, the laser radiation intensity needs $I_0 \geq 10^9$ W/cm^2 (for an Al target). The required electron concentration due to emission from the surface, as well as due to vapor ionization by electrons, can only be obtained at this kind of intensity.

Since the bremsstrahlung absorption coefficient rapidly grows with the decreasing of electromagnetic field frequency ($\sim 1/\omega^2$), the use of MR at $\omega_m \ll \omega_0$ frequency should be expected to result in a more efficient electron heating. Yet, it should be remembered that at $\omega_m < \omega_p$ or

$$\omega_m < \sqrt{4\pi e^2 n_e/m}. \tag{11}$$

MR can no longer penetrate the plasma region. To avoid this happening before the critical concentration n_e^* has been achieved, from Eqs. (10) and (11) we obtain that ω_m must satisfy the condition

$$\omega_m^2 \geq 3.2\cdot 10^9\frac{A_{21}^*}{K_{21}}. \tag{12}$$

However, increasing ω_m far beyond the limit specified in inequality (12) is not reasonable as this would noticeably reduce the MR absorption.

3. Results

Figures 2 and 3 show the results of numerical calculations obtained using the mathematical model (Eqs. (1)–(9)) for the aluminum surface exposed to square laser ($\lambda \approx 1.06$ μm) and

MR pulses. The model is concerned with the excited state 4S only while the ground state 4P embraces the $4P_{1/2}$ and $4P_{3/2}$ levels with a total statistic weight of $g_1 = 6$. The coefficient of laser radiation absorption by the target is $r_c \approx 0.05$.[13] Figure 2 illustrates the results obtained for the following conditions: $J_0 = 50$ MW/cm^2, $J_m = 1$ kW/cm^2, the laser pulse duration $\tau_0 = 3$ μs, the MR pulse duration $\tau_m = 3$ μs, and $\omega_m = 10^{11}$ s^{-1}.

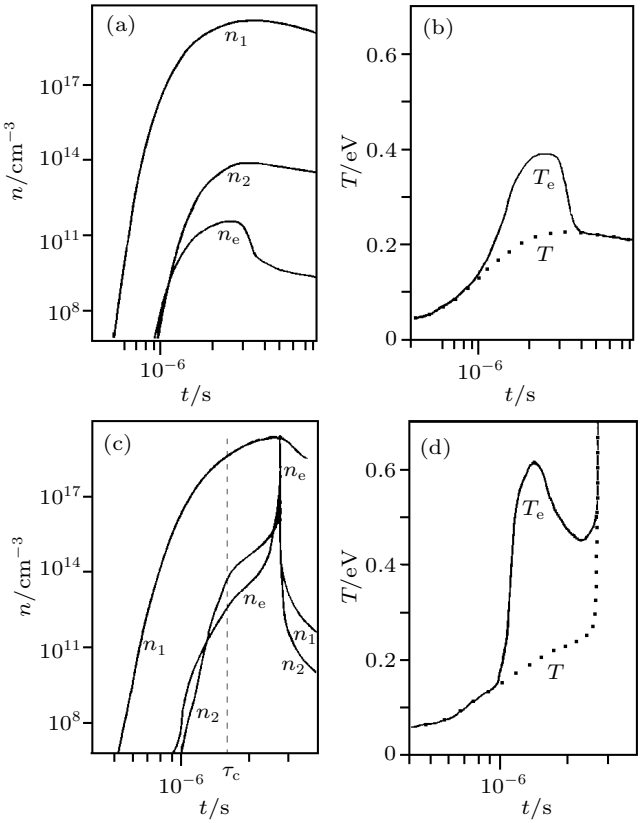


Fig. 2. Dynamics of the particle concentration and temperature under applied laser radiation only (a) and (b) and under laser and microwave irradiation (c) and (d).

Figure 3 illustrates the results obtained for the conditions: $J_0 = 200$ MW/cm^2, $\tau_0 = 0.5$ μs, $J_m = 100$ kW/cm^2, $\tau_m = 0.3$ μs, $\omega_m = 10^{12}$ s^{-1} and the exposure to MR starting 0.2 μs after commencement of irradiation by laser pulses.

As one can see from Figs. 2(a), 2(b), 3(a), and 3(b), the vapors of the target resulting from laser irradiation remain weakly ionized in the absence of MR, and the formation of electrons is predominantly due to emission from the surface. Initially, when vapor concentration is low, the heating of electrons by the laser radiation is insignificant. The temperature of electrons is equal to that of vapor and is determined by the surface temperature (Figs. 2(b) and 3(b)). The laser radiation absorption grows with the increase of vapor concentration and the temperature of the electrons also goes up, correspondingly. The loss of electron energy mostly occurs because of vapor expansion and energy transfer to atoms via elastic collisions. Elevated electron temperatures open up a new channel for electron energy losses associated with excitation of atoms followed by their spontaneous decay. These losses further impede (at moderate laser intensities) the heating of electrons and stabilize their temperature at the values (Figs. 2(b) and 3(b)) insufficient for the atoms to be ionized by electron impact. Hence, the electron concentration within the pulse duration fails to reach the value of n_e^*, above which the energy expended on excitation of atoms returns to the electrons.

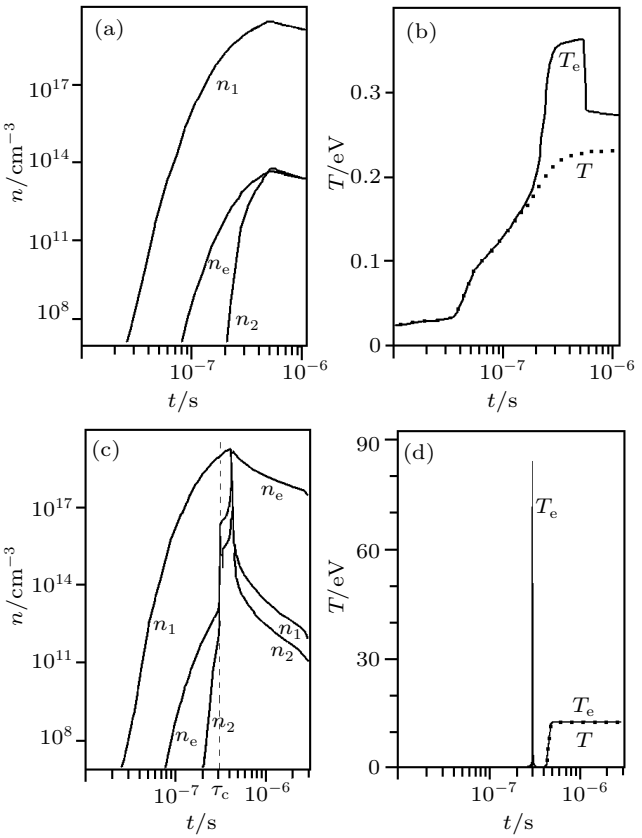


Fig. 3. Dynamics of the particle concentration and temperature under applied laser radiation (a) and (b) and under combined laser and microwave irradiation (c) and (d).

The complementary application of MR and laser radiation lead to a faster heating of electrons enabling the finding of the atom excitation "threshold" and the reaching of the temperature required for electron ionization of atoms. Hence, the concentration of electrons keeps growing until it reaches the critical value

$$n_{cr} = \frac{m \cdot \omega_m^2}{4\pi e^2}, \tag{13}$$

(following from inequality (11)), above which MR can no longer penetrate the plasma region (in the figures, this instance is indicated by a vertical dashed line $t = \tau_c$). The electrons are further heated by laser radiation only. Provided $n_{cr} > n_e^*$ (see Eq. (10)), less electron energy is wasted on the excitation of atoms, which allows the temperatures required for a subsequent full ionization of atomic vapors to be obtained by heating electrons with laser radiation. Once the ionization reaches ~ 0.001 (for instance, in the former case this happens at time $t \approx 2.5$ μs), the bremsstrahlung absorption coefficient drastically increases because the elastic electron–ion

collisions, having fairly large cross sections compared with electron–atom collisions, become dominant. This facilitates a further increase in the heating rate of electrons and ionization of vapors. It should be noted that full ionization of vapors results in plasma shielding of the target and, hence, a smaller portion of laser radiation can reach the surface of the target. For example, for the first mode in Fig. 2(a) one can see that without the stimulating effect of MR, when the vapor is weakly ionized, the vapor concentration maximizes by the end of the laser pulse. However, when vapors are fully ionized (Fig. 2(c)), starting from time $t \approx 2.7$ μs the total plasma concentration rapidly drops off before the laser pulse is over. This happens because of the growing thickness of the plasma layer, enhanced absorption of plasma by the laser radiation, which hinders the heating of the target surface by this radiation. Indeed, for the plasma concentration $n_e \sim 10^{19}$ cm^{-3}, electron temperature $T_e \approx 1$ eV and the thickness of the plasma layer obtained in this mode $H_1 \approx 0.3$ cm, its optical thickness for the laser radiation is about 100. The same goes for the mode depicted in Fig. 3 where the full ionization and the radiation "cutoff" happen at time $t \approx 0.41$ μs, after which the total concentration again is observed to drop off before the laser pulse is over. With the thickness of the plasma layer in this mode being $H_1 \approx 0.06$ cm, its optical thickness is obtained to be ~ 20.

The numerical estimates have also shown that under the conditions presented in Fig. 2 but with the frequencies being $\omega_m = 10^{10}$ s^{-1} and 10^{12} s^{-1} full vapor ionization also does not happen. This may be related to the early "cutoff" of MR in the case of $\omega_m = 10^{10}$ s^{-1} and with the low absorption coefficient for the given intensity J_m in the case of $\omega_m = 10^{12}$ s^{-1}. Similarly, for the same reasons, no full ionization is observed at $\omega_m = 10^{11}$ s^{-1} and 10^{13} s^{-1} under the conditions shown in Fig. 3.

Compared the obtained numerical estimates with the theoretical findings discussed above, we will have mean values $K_{21} \sim 3 \times 10^{-8}$ s^{-1} and $A_{21} \approx 1.2 \times 10^{8}$ s^{-1} for the transitions in aluminium atoms 3P–4S ($\lambda \approx 0.4$ μm). The numerical calculations indicate that the concentration of normal atoms $n_1 \sim 10^{19}$ cm^{-3} is achieved within the laser pulse duration in both modes. The gas layer thickness is $H_1 \approx 0.3$ cm in the former case, and $H_2 \approx 0.06$ cm in the latter case. Since resonance broadening of absorption line at the given transition plays a dominant role at the given concentration, we find the absorption cross section to be $\sigma \sim 1.4 \times 10^{-13}$ cm^2. We next find the effective coefficient A^*_{21} of spontaneous decay and estimate n^*_e from Eq. (10): $A^*_{21} \approx 1.5 \times 10^5$ s^{-1}, $n^*_e \approx 5 \times 10^{12}$ cm^{-3} for the first mode, and $A^*_{21} \approx 3.3 \times 10^5$ s^{-1}, $n^*_e \approx 1.1 \times 10^{13}$ cm^{-3} for the second mode. From inequality (12) we then find the lowest permissible value of ω^*_m for which $n^*_e \leq n_{cr}$ and obtain $\omega^*_m \sim 1.0 \times 10^{11}$ s^{-1} for the first mode and $\omega^*_m \sim 2 \times 10^{11}$ s^{-1} for the second mode. That is, the MR frequencies ensuring the full ionization of vapors that we chose for our numerical simulation are in fairly good agreement with the theoretical findings.

4. Conclusions

We have shown that with a complementary use of low-intensity MR, full ionization of target vapors can be achieved at laser radiation intensities at least 1÷2 orders of magnitude lower than in the case without MR. The role of MR is to heat up electrons and maintain their concentration at the levels such that de-excitation of atoms is predominantly due to electron impact. Also, the laser intensity must be chosen such that a sufficient vapor density is produced within the period of irradiation to enable a substantial increase in the effective lifetime of an excited atom ($1/A^*_{21}$). Application of this phenomenon is the most advantageous for visible laser radiation. With the UV radiation, accelerated plasma formation (even without MR radiation) can be achieved due to two-photon ionization of normal atoms and one-photon ionization of excited atoms.[9,14] In the case of IR radiation (CO_2 laser), the bremsstrahlung absorption coefficient is considerably higher and, hence, the heating of electrons at the same intensities is more efficient than in the case of visible radiation.

References

[1] Ready J F 1971 *Effects of High-Power Laser Radiation* (New York: Academic Press)

[2] Veiko V P, Smirnov V N, Chirkov A M and Shakhno E A 2013 *Lazernaya Ochistka v Mashinostroenii i Priborostroenii* (Sankt-Petersburg: NIU ITMO) (in Russian)

[3] Gavrilyuk A P, Shaparev N Ya and Yakubailik O E 1993 *Quantum Electronics* **23** 718

[4] Knight C J 1979 *AIAA Jornal* **17** 519

[5] Rosen D I, Mitteldorf J, Kothandaraman G, Pirri A N and Pugh E R 1982 *J. Appl. Phys.* **53** 3190

[6] Majukin V I and Samokhin A A 1987 *Mathematical Modeling: Nonlinear Differential Equations in Mathematical Physics* (Moscow: Nauka) (in Russian)

[7] Biberman L M, Vorobév V S and Yakubov I T 1987 *Kinetics of Nonequilibrium Low-Temperature Plasmas* (New York: Springer) Chap. 3

[8] Raizer Yu P 1978 *Laser-Induced Discharges* (New York: Consultants Bureau USA) Chap. 1

[9] Gavrilyuk A P, Shaparev N Ya and Yakubailik O E 1994 *High Power Laser and Particle Beams* **6** 91 (in Chinese)

[10] Bowe P, Conway J, Dunne P, McCormack T and O'Sullivan J 1999 *J. Appl. Phys.* **86** 3002

[11] McCormack T and O'Sullivan G 1999 *Review of Scientific Instruments* **70** 2674

[12] Hora H 1981 *Physics of Laser Driven Plasmas* (New York: John Wiley and Sons) Chap. 6

[13] Prohorov A M, Konov V I, Ursu I and Mihailesku I N 1988 *Interaction of Laser Radiation with Metals* (Bucuresti: Acad. Edit,; Moscow: Nauka) Chap. 1

[14] Amoruso S 1999 *Appl. Phys. A* **69** 323